Coherent Acoustic Phonons and Ultrafast Carrier Dynamics in Hetero-Epitaxial BaTiO$_{3}$-BiFeO$_{3}$ Films and Nanorods

Journal:	*Journal of Materials Chemistry C*
Manuscript ID	TC-ART-03-2019-001584.R4
Article Type:	Paper
Date Submitted by the Author:	04-Oct-2019
Complete List of Authors:	Mudiyanselage, Rathsara; Virginia Tech Magill, Brenden; Virginia Tech, Burton, John; Virginia Tech Miller, Moira; Virginia Tech Spencer, Joseph; Virginia Tech McMillan, Kiara; Virginia Polytechnic Institute and State University Khodaparast, Giti; Virginia Tech, Department of Physics Kang, Han Byul; Virginia Polytechnic Institute and State University, Materials Science and Engineering; Virginia Tech Kang, Min-Gyu; Virginia Polytechnic Institute and State University, Maurya, Deepam; Virginia Tech, Department of Materials Science Priya, Shashank; Virginia Tech, Department of Materials Science and Engineering Holleman, Jade; Florida State and National High Magnetic Field Labs McGill, Stephen; National High Magnetic Field Laboratory, Stanton, Christopher; University of Florida, Physics

SCHOLARONE™
Manuscripts

Coherent Acoustic Phonons and Ultrafast Carrier Dynamics in Hetero-Epitaxial BaTiO$_3$-BiFeO$_3$ Films and Nanorods

Rathsara R. H. H. Mudiyanselage[1†], Brenden A. Magill[1†], John Burton[1],

Moira Miller[1], Joseph Spencer[1], Kiara McMillan[1], Giti A. Khodaparast[1*],

Han-Byul Kang [2†], Min Gyu Kang[2], Deepam Maurya[2], Shashank Priya[2,3],

Jade Holleman[4,5†], Steve McGill[4,5], and Christohper J. Stanton [6]

[1]*Department of Physics, Virginia Tech, Blacksburg, VA 24061, USA,[*]

[2]*Center for Energy Harvesting Materials and Systems (CEHMS)*

and Bio-inspired Materials and Devices Laboratory (BMDL),

Virginia Tech, Blacksburg, VA 24061, USA,

[3]*Materials Research Institute, Penn State, University Park, PA 16802, USA,*

[4]*National High Magnetic Field Laboratory,Tallahassee, FL 32310, USA,*

[5]*Physics Department, Florida State University, Tallahassee, FL 32306, USA,*

[6]*Department of Physics, University of Florida , Gianesville, FL 32611, USA*

(Dated: October 4, 2019)

Abstract

The desire for multifunctional devices has driven significant research toward exploring multiferroics, where the coupling between electric, magnetic, optical, and structural orders parameters can provide new functionality. While $BiFeO_3$ is a well studied multiferroic, recent research has shown that the addition of $BaTiO_3$ can improve the material properties. In this study, we perform time resolved differential reflectivity measurements of $(1-x)BaTiO_3 - (x)BiFeO_3$, with x = 0.725 epitaxial films grown on a Lanthanum Strontium Manganite (LSMO) layer with a Strontium Titanate (STO) substrate, and $BaTiO_3$-$BiFeO_3$ nano-rods grown on Pt/Si. Our time resolved measurements can be used to probe dynamical properties on picosecond time scales. Information obtained is vital towards the design and understanding of high speed devices that incorporate multiferroic materials. We find that the contribution to the transient reflectivity response of a $BaTiO_3$-$BiFeO_3$ film due to carrier dynamics can be quantitatively explained by the diffusion of the photoexcited carriers away from the surface and that the ambipolar diffusion constant is below 1-2 cm^2/s. At low temperature and for thicker films, in addition to a response from carrier dynamics, we also observed oscillations in the transient reflectivity with periods of 30-37 ps. We attribute these oscillations to propagating coherent acoustic phonons in the films. In the $BaTiO_3$-$BiFeO_3$ nano-rods samples only, we observed an additional oscillation with frequency in the range of 8 GHz. This is close to a theoretically predicted magnon frequency, but the strength of this oscillation only had a very weak magnetic field dependence. Another explanation for this feature could be multiple reflections of the acoustic phonons at the Pt interfaces (due to the large acoustic impedance mismatch).

---

* Corresponding author: khoda@vt.edu, † Authors with equal contributions.

I. Introduction

The desire to create monolithic multifunctional devices has driven significant research toward exploring multiferroics, where the coupling between electric, magnetic, optical, and structural order parameters[1–5], can provide new functionality. Multifunctionality in a single material allows for the development of novel devices such as: low energy and high speed computer memory elements[6,7], high efficiency photoelectric devices[8], conversion of photons from optical to THz[9,10] frequencies, and new electronic architectures[11]. Multiferroics have potentials for many applications[2,3,12–16], such as ultrafast non-volatile ferroelectric memory[14,17], spintronic devices[15], and energy harvesting.[18,19] Furthermore, strained multiferroic materials and their heterostructures have also the potential for phononic device applications in which photons and phonons can couple strongly.[20–26]

Among the various multiferroics, bismuth ferrite ($BiFeO_3$) is one of the most studied lead-free material systems. However, it suffers from decreased ferroelectric polarizability which results from large leakage currents mainly due to the presence of multivalent Fe ions and oxygen vacancies.[13–18] We have shown earlier[2] that the addition of $BaTiO_3$ to $BiFeO_3$ reduces the conductivity of the mixture which decreases the leakage current, potentially allowing for a better multiferroic material. A similar observation was reported by Park *et. al*[27]. In both studies, a wide range of material compositions were synthesized. This solid solution approach has the advantage of enhancing the magneto-electric (ME) properties. In our previous study[2], $(1-x)BaTiO_3$-$(x)BiFeO_3$ admixtures with x between 0.725 and 0.750, were demonstrated to have a larger ME coupling compared to $BiFeO_3$ due to active spin modulation of the Fe-O-Fe bond.[2,27] We also recently reported room temperature ferromagnetic resonance in 80 nm thick $BaTiO_3$-$BiFeO_3$ grown on 100 nm thick lanthanum strontium manganite (LSMO), where this hybrid heterostructure was found to show small Gilbert damping of 0.004.[28] This fact offers opportunities for employing this material system for a spin transfer where potentially a spin current can be generated without the existence of charge current in the $BaTiO_3$-$BiFeO_3$ layer.[28]

In this paper, we use time resolved pump-probe differential reflectivity measurements (TRDR) to study our $(1-x)BaTiO_3$-$(x)BiFeO_3$ admixtures. We studied several different $(1-x)BaTiO_3$-$(x)BiFeO_3$, $x = 0.725$ films as well as nano-rods. Our studies provide information primarily on generation and propagation of acoustic coherent phonons (CPs) (sound veloci-

ties and indices of refraction) and to a lesser extent on the dynamics of photo-excited carriers (diffusion constants). For carrier dynamics, pump-probe studies of the transient reflectivity allow probing the time scales for carrier diffusion, inter-band scattering, carrier trapping, and band to band recombination of the photoexcited electrons and holes.[29] Compared to our previous studies on $(1-x)BaTiO_3$-$(x)BiFeO_3$ poly-crystalline structures reported in[30,31], these new films studied here, have the advantage of lower disorders and a well-defined layered structure. In addition to the films, we also examined $BaTiO_3$-$BiFeO_3$ *nano-rods*, in which the smaller substrate clamping effect is expected to lead to stronger mechanical coupling and thereby to higher piezoelectricity and magnetostriction than in the films.[1]

$BiFeO_3$ is G-type antiferromagnetic (AFM), where within the (111) plane, the magnetic spins are ferromagnetically aligned, while between the adjacent (111) planes, they are anti-ferromagnetically aligned. The Dzyaloshinskii-Moriya interaction produces a weak canting moment, thereby leading to weak in-plane FM.[32] In bulk (as opposed to the films) this orientation is modulated to a spiral spin structure, whose AFM vector has a wavelength of 62-64 nm, resulting in local weak AFM in $BiFeO_3$.[33,34] Several investigations have shown that an inherent net magnetization can be achieved if one can suppress the spiral spin structure[32–37].

This spiral structure is believed to be suppressed in nanostructures, such as nanoparticles, nanotubes, and nano-wires. This is our motivation for studying the nano-rods. Recent approaches show enhanced magnetization correlated with the decreasing of the nano-rod diameter below the wavelength of the spiral order.[34] Reducing the dimensionality from the films to nano-rods (quasi-1 dimensional) was expected to enhance the possibility of detecting coherent magnons in the nano-rods.[38] For antiferromagnet or ferromagnet magnons, one would expect an increase in frequency with applied magnetic field which motivated us to probe the magnetic field dependence of the time resolved dynamics in our studies. We also note that multiferroics networks of $BiFeO_3$ nano-rods[39] displayed enhanced magnetism compared to the bulk $BiFeO_3$, arrays of $BiFeO_3$ quantum dots[7] exhibited bipolar resistive switching, and composite rod-bulk structures[40] demonstrated enhanced ferroelectricity. This also is a motivation for studying the nano-rods.

II.   Sample Preparation and Characterization

A.   BaTiO$_3$-BiFeO$_3$ Films

The characteristics and geometry of the samples investigated in this paper are summarized in Table I and we provide a brief introduction to the growth procedures. The lattice mismatch of the BaTiO$_3$-BiFeO$_3$ with respect to the strontium titanate, SrTiO$_3$ (STO) substrate and LSMO film is small which allows it to be epitaxially grown on both materials. Hetero-epitaxial BaTiO$_3$-BiFeO$_3$/LSMO thin films were grown on (001) oriented STO substrates by off-axis RF magnetron sputtering. Prior to the film deposition, the surface of the STO substrates was treated by buffered oxide etchant (BOE) and subsequently annealed at 900°C under an O$_2$ atmosphere to make a Ti-terminated surface. First, the LSMO thin film was deposited on the Ti-terminated STO substrate at 600 ^{o}C under 5 mTorr of pressure with 8:2 O2:Ar gas ratio and 4.93 W/cm^2 of RF power. The BaTiO$_3$-BiFeO$_3$ thin film was grown on the epitaxial LSMO thin films at 400 ^{o}C using an in-situ deposition under the same RF power and pressure with 1:9 O2:Ar gas ratio.

Cross-sectional scanning electron microscopy (SEM) image for one of the samples (Sample 4), shows the BaTiO$_3$-BiFeO$_3$/LSMO thin film grown on the STO (Fig. 1(a)). The ferromagnetic (FM) and FE characteristics of this sample are presented in Fig. 1(b). The temperature dependent magnetization of the BaTiO$_3$-BiFeO$_3$/LSMO at 0.5 Tesla, indicates that the film has non-zero magnetization at room temperature. The inset in Fig. 1(b) shows the FE polarization-electric field (P-E) curve of the BaTiO$_3$-BiFeO$_3$ film. It shows the typical and unambiguous FE characteristics. The crystal structures of the epitaxial LSMO film and hetero-epitaxial BaTiO$_3$-BiFeO$_3$/LSMO thin films grown on (001) oriented STO substrates were confirmed through X-ray diffraction (XRD) analysis. The films were found to be epitaxially grown along the c-axis of the STO substrate without any secondary phases, as illustrated in Fig. 1(c). The peak splitting corresponding to (001) and (002) planes, indicates that the film is grown with the rhombohedral phase as reported in reference 2. Our previous X-ray diffraction of the BaTiO$_3$-BiFeO$_3$ poly-crystalline film also showed that the film was in a pure perovskite phase and no pyrochlore phase was observed.[31]

Figure 1(d) shows phi-scan XRD patterns of BaTiO$_3$-BiFeO$_3$/LSMO epitaxial films. Azimuthal phi-scans of BaTiO$_3$-BiFeO$_3$ and LSMO films show in-plane epitaxy with a cube-

on-cube epitaxial relation. The $(1-x)BaTiO_3 - (x)BiFeO_3, x = 0.725$ used in this work, is a solid solution with the rhombohedral phase which has lattice parameter of a=3.982 Å, rhombohedral distortion angle of 89.99^o and unit cell volume of 63.31 $Å^3$ in its bulk form.

TABLE I. Samples studied in this work. Note: The labels BTO-BFO refer to BaTiO$_3$-BiFeO$_3$. *In the case of the nano-rods, the LSMO layer refers to nano-sphere arrays.

Sample	Thickness BTO-BFO (nm)	Thickness LSMO (nm)	STO Orientation	Structure
1		100	(001)	LSMO/STO
2	80	100	(001)	BTO-BFO/LSMO/STO
3	80	40	(001)	BTO-BFO/LSMO/STO
4	660	100	(001)	BTO-BFO/LSMO/STO
5 (nano-rods)*	500			BTO-BFO/LSMO/Pt/Si

B.   BaTiO$_3$-BiFeO$_3$ nano-rods

As shown in Fig. 2(a), 0.275BaTiO$_3$-0.725BiFeO$_3$ nano-rods were grown on 20 nm size LSMO seeds. These nano-sphere seeds were patterned on top of Pt coated Si (100) substrate through polymer nano-template method followed by RF sputtering, at 400^oC. The spherical LSMO seeds drive vertical growth of the BaTiO$_3$-BiFeO$_3$ nano-rods due to the minimization of overall surface energy. The nano-rod arrays were synthesized with ∼200 nm diameter and ∼500 nm height, as shown in the side view image in Fig. 2(b). This method for growing BaTiO$_3$-BiFeO$_3$ nano-rods is similar to the techniques employed for synthesizing PbZr$_{0.52}$Ti$_{0.48}$O$_3$ (PZT) nano-rods and the details can be found in Ref. [1].

Through SEM measurements, we found that the BaTiO$_3$-BiFeO$_3$ nano-rods (Fig. 2(b)) exhibit close-packed structure[1] and have a nearly homogeneous diameter and height (these closed-packed microstructures are homogeneous up to 3-inch wafer scale). From XRD measurements, the nano-rod arrays were found to be single perovskite phase without any secondary phases such as pyrochlore phase (A$_2$B$_2$O$_7$), as shown in Fig. 2(d). The XRD pattern also indicates that the nano-rods are poly-crystalline. However, based on previous results on
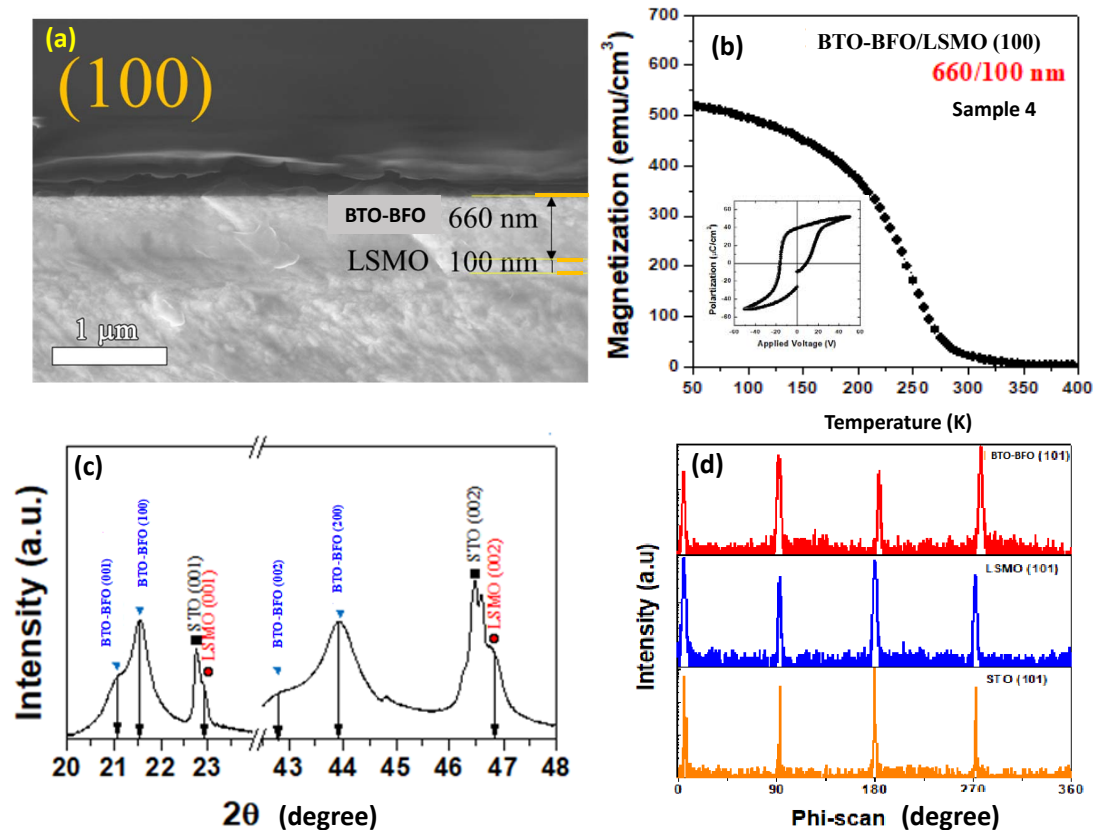
FIG. 1. (a) SEM image of the layer structure of the $BaTiO_3$-$BiFeO_3$ film investigated in this study (sample 4). (b) The magnetization as a function of temperature at 0.5 Tesla, and the inset shows FE loop at RT demonstrating the multiferroic nature. (c) The XRD of sample 4 shows a single phase for the $BaTiO_3$-$BiFeO_3$ film. (d) Here we present, (101) Phi-scan XRD patterns of $BaTiO_3$-$BiFeO_3$/LSMO epitaxial layers grown on (100) STO substrate (sample 4). The films are grown through (001) direction and the phi scan was performed with (101) space to evaluate the epitaxial quality. Note: The labels BTO-BFO refer to $BaTiO_3$-$BiFeO_3$.

$PbZr_{0.52}Ti_{0.48}O_3$ using the same growth procedure[1], we expect that a single nano-rod, is a single crystal but each nano-rod has different crystal orientation, which imparts the overall poly-crystalline nature.

The difference in the thermal expansion coefficient between the thin film and substrate usually can create internal stress when they are synthesized at high temperature and then cooled down to room temperature. This thermal stress results in the preferred orientation of the thin films because the thin film is strongly clamped on the substrate during the
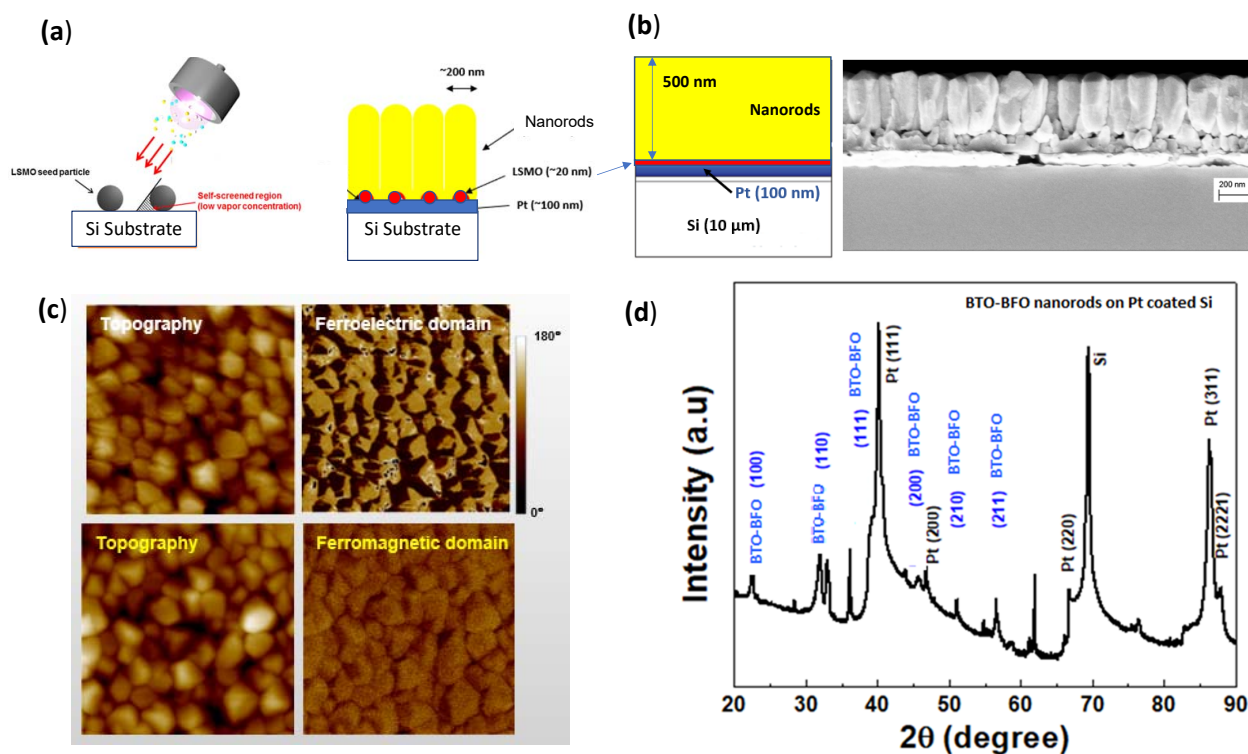
FIG. 2. (a) Schematic of the nano-rods growth on spherical LSMO seed particles. The seeds were arranged using polymer nano-sphere coating followed by LSMO deposition. (b) A side view SEM image of the nano-rods on 100 nm Pt film. The red region refers to the LSMO spherical seed particles. (c) Atomic Force Microscopy images of $BaTiO_3$-$BiFeO_3$ nanorod arrays grown on Pt-coated Si substrate displaying topography, FE, and FM domains. (d) XRD patterns of $BaTiO_3$-$BiFeO_3$ nano-rod arrays. Note: The labels BTO-BFO refer to $BaTiO_3$-$BiFeO_3$.

cooling process. The nano-rods show randomly oriented XRD peaks like bulk materials. This indicates that thermal stress is not induced into the sample during the cooling process and the nano-rods overcome the substrate clamping effect. This is significant because the substrate clamping effect in thin films significantly hinders the mechanical coupling of the ferroic orders, such as piezoelectricity in the FE materials, and magnetostriction in the FM

materials. This effect occurs because the film is chemically bonded on the rigid substrate, which limits the mechanical movement of the thin film, under external excitation such as applied electric or magnetic field.[1]

III. Results and Discussion

Time-resolved differential reflectivity spectroscopy was performed on the epitaxial $BiFeO_3$ films and nanorods discussed above. Our results show a decay in $\Delta R/R$ with time which we attribute to the dynamics of the photoexcited carriers.[41–43] In our signals, we observe clear oscillations and "bumps" and we associate them to the generation of coherent longitudinal acoustic (LA) phonons near the surface of the sample and their subsequent propagation into the sample and other layers.[44]

We previously[30,31] performed time-resolved measurements on *polycrystalline* $BaTiO_3$-$BiFeO_3$ where the second harmonic generation nano-imaging revealed disordered but distinct ferroelectric domains. In a two color pump/probe scheme (400/800 nm), we observed transient reflectivity responses and described the dynamics using a double exponential function, representing fast (2-7 ps) and slow (a few hundred ps) components.[30] We attributed the relaxation process to phonon-mediated as well as the diffusion of the photoexcited carriers. We also attribute an oscillation in $\Delta R/R$ (in GHz range) to the transverse acoustic phonons.[31] Furthermore, we observed a small magnetic field dependence in the amplitude of the transient reflectivity.[31] The electronic energy relaxation of polycrystalline $BiFeO_3$, deposited on STO and ytrrium stabilized ZrO2 (YSZ) substrates, were also studied using a two color pump/probe spectroscopy (400/800 nm).[41] In their work, the hot electrons were identified to decay with two different characteristic time scales. The fast process was attributed to scattering of electrons with lattice-vibration modes, and the slow one to the spin-lattice thermalization.

In this study, we improved the quality of our samples by making *films*, which had smoother, well-defined layers which allow us to better interpret the optical data. We performed pump-probe reflectivity measurements and our laser source was a Coherent amplified Ti:sapphire oscillator with a repetition rate of 1 kHz, a wavelength of 800 nm, and a pulse duration of 100 fs with ~ 1 W output power. We used 90% of the output power for the pump path and the pump pulses were delayed respect to probe using a tunable delay line. The

pump pulses were frequency doubled to 400 nm via a 0.5 mm thick BBO crystal generating pulses with a maximum power of 2 mW . The probe beam of 800 nm, had a spot size of $150 - 200$ μm with the pump being slightly larger ($\sim$ 250-300 μm). For the range of the pump powers used in this work (0.5-2 mW), we can estimate the pump fluence to vary from ~ 0.7 to 4 mJ/cm^2. For the probe pulses, the power was fixed at (~ 10 μW), corresponding to a fluence of ~ 30 $\mu J/cm^2$. Both beams were focused on the samples using lenses. At room temperature, in order to increase the signal to noise ratio, the modulation frequency of the laser (1 KHz) was used to trigger the Lock-in amplifier and at 100 K we modulated the pump pulses using a chopper at 211 Hz.

A.   Carrier Relaxation Dynamics in BaTiO$_3$-BiFeO$_3$ Films

Figure 3(a) presents examples of the observed TRDR in our two color pump/probe scheme at RT, for sample 2 at different pump powers. For comparison in Fig. 3(b), the TRDR on an LSMO film (sample 1) shows no response (or at least a much weaker one) from just this layer.
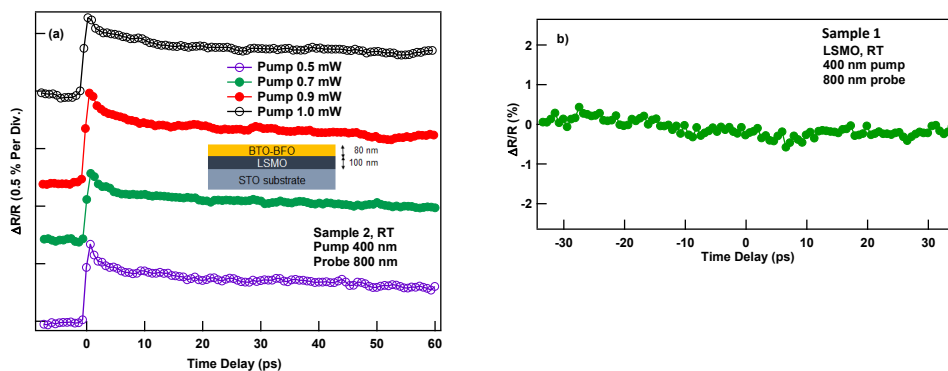

FIG. 3. (a) TRDR of 80-nm thick BaTiO$_3$-BiFeO$_3$ (sample 2), measured at room temperature with the pump wavelength at 400 nm and probe at 800 nm, for different pump powers. The traces are offset for clarity and we refer to TRDR as the change in the transient reflectivity at positive time delay respect to the negative time delay. (b) TRDR on an LSMO (sample 1) film showing no detectable pump-induced response. Note: The labels BTO-BFO refer to BaTiO$_3$-BiFeO$_3$.

The observed decay in the differential reflectivity can be attributed to the dynamics of

the photoexcited carriers near the surface.[29] The short absorption depth of the 400 nm pump pulse leads to a nonuniform photoexcited carrier density. The carrier contribution to the differential reflectivity[29] is proportional to the change in the *surface* carrier density in a given band, divided by the effective mass of the given band, and summed over all bands and is given by:

$$\frac{\Delta R}{R} \sim -\left(\sum_i \frac{\Delta N_i}{m_i}\right). \qquad (1)$$

Note that a differential reflectivity measurement provides different information than a differential transmission measurement. In a differential transmission experiment, one measures the total number of carriers throughout the entire sample, at a *specific energy state* in a given band, that block the absorption of the probe pulse. In contrast, in the differential reflectivity, one only measures the carriers *near the surface*. In addition, the differential reflectivity depends only on the band in which the carrier is residing and is not sensitive to the specific energy state. For instance, phonon scattering from a given energy state would produce a change in the differential transmission signal, but would not produce a change in the differential reflectivity unless the carrier scattered into a *different* band with a *different* effective mass.

Changes in the differential reflectivity due to the carrier dynamics can occur for a variety of reasons.[45] These include: 1) scattering of carriers at the surface to *different* bands with *different* masses; 2) recombination of photoexcited carriers (either through surface defects or band to band transitions); and 3) diffusion of carriers away from the surface. In addition, we note that the carriers can also influence the *band gap renormalization* which can affect the differential reflectivity signal. We do not consider band gap renormalization here.

The absorption depth of the 400-nm light in $BiFeO_3$ is 32 nm, whereas $BaTiO_3$ is transparent[46] at this wavelength. The absorption depth of the solid solution is therefore estimated to be in the range of 35-45 nm, much shorter than even our thinnest film. We therefore believe that the observed reflectivity responses are dominated by carrier diffusion away from the surface. We express the initial (t=0) depth distribution (z) of the photoexcited carriers in the sample by $N(z, t = 0) = N_0 e^{-\alpha z}$ where N_0 is the initial surface carrier density and α is the absorption coefficient. Then the carrier distribution at t>0, z>0 can

be described by:

$$N(z = 0, t) = N_o e^{\alpha^2 D t} \left[\text{erfc} \left(\frac{\alpha D t}{\sqrt{Dt}} \right) \right]. \tag{2}$$

Here D is the diffusion constant, and erfc is the complementary error function. Note that $1/\alpha^2 D$ has units of time and defines the time scale for the diffusion from the surface.[29] For small $t \ll 1/(\alpha^2 D)$ it decays as

$$N(0, t) \approx N_0 \left(1 - \frac{2}{\sqrt{\pi}} \alpha \sqrt{Dt} \right). \tag{3}$$

This tells us that N_0 does not decay exponentially with a single time constant. (See appendix B of Ref. [29]). Instead, the decay of N_0 can be conveniently expressed with a time-dependent *instantaneous* decay rate $\gamma(t)$, which is defined by:

$$\frac{d}{dt} N(0, t) \equiv -\gamma(t) N(0, t). \tag{4}$$

We can rewrite equation 4 as:

$$\gamma(t) \equiv -\frac{1}{N(0, t)} \frac{dN(0, t)}{dt} = -\frac{d \ln(N(0, t))}{dt}. \tag{5}$$

For small t, for a diffusive process, by using Eq. 5 and 3, this rate is given by: $\gamma(t) = \alpha \sqrt{\frac{D}{\pi t}}$. Note, that this varies rapidly at short times and in fact, at $t = 0$ is infinite.
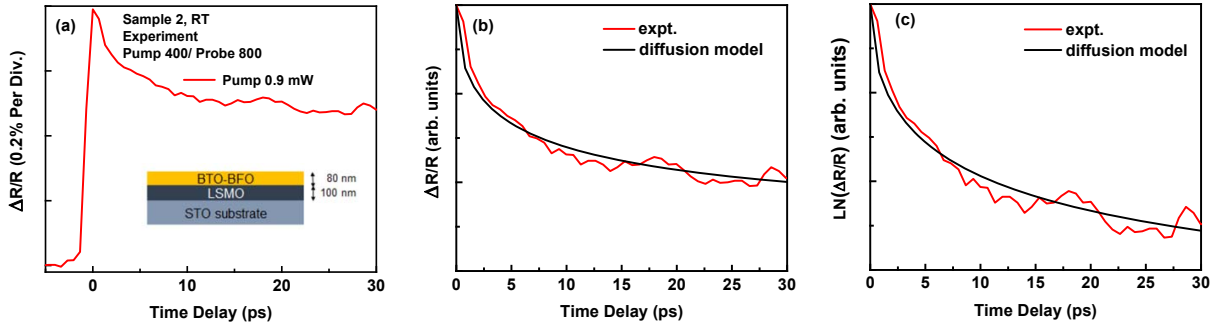

FIG. 4. (a) The experimental differential reflectivity ($\Delta R/R$) of sample 2 at room temperature at pump power of 0.9 mW. Experimental reflectivity trace scales (red) compared with calculated $N_0(t)$ (black) from the diffusion model, assuming $1/\alpha^2 D = 10$ ps, plotted in the linear (b) and the natural log scale (c).

The model to describe surface carrier density $N_0(t)$ can reasonably reproduce the experimental data in Fig. 4. In doing so, we find that we get reasonable agreement if we set

our diffusion time scale, $1/\alpha^2 D = 10\ ps$. This would give a diffusion constant 1-2 cm^2/s, more than an order of magnitude less than the ambipolar diffusion coefficient for 400 nm photo-excitation in GaAs[47] which was estimated to be between 15 and 75 cm^2/s and seems plausible, given the disorder in the solid solution. In actuality, the diffusion coefficient could be even smaller than this since other processes can contribute to the decay of the signal as discussed above.

The relaxation mechanisms in our samples are different than those found in several recent studies in similar systems. In a study by Doig $et.\ al$[38] a two-color time-resolved pump/probe reflectivity (400/800 nm) of rhombohedral-like-BFO film on $LaAlO_3$ also showed non-exponential decay, where the initial relaxation was attributed to the phonon emission and the slower recovery to the incoherent acoustic emission, spin lattice coupling or radiative recombination. Chen $et.\ al.$[44] also probed the reflectivity dynamic of $BiFeO_3$ thin films in a two-color pump/probe where the observed excitation was triggered by transferring the electrons from 2p valence band of O to p conduction band of Bi. In this study, the number of the excited electrons generated by this non-thermal process was related to the amplitude of $\Delta R/R$. The cooling process was related to relaxation of high-energy electrons accumulated in the p conduction band of Bi, through the emission of longitudinal-optical (LO) phonons within several picoseconds. The ultrafast photo-induced absorption spectroscopy, in a single crystal of $BiFeO_3$ using sub-100-fs optical pulses in the near-infrared and ultra-violet ranges, was reported by Matsubara $et.\ al.$[42] In their study, It was concluded that the dominant transient absorption originated from the two-photon absorption process and collective electron-electron in addition to electron-phonon scattering, were the dominating relaxation mechanism.

B. Coherent Phonons in $BaTiO_3$-$BiFeO_3$ Film at Low Temperature

In this section, we investigate the oscillations in the TRDR of the $BaTiO_3$-$BiFeO_3$ films at low temperature which are associated with generation and propagation of coherent acoustic phonons. An example for sample 3 is shown in Fig. 5(a) for external fields up to 10 Tesla at 100 K. The pump was 400 nm (with the power of $\sim$ 2 mW) and the probe, 800 nm. We note that there is an additional feature at 16-18 ps, which manifests itself as a "bump" in the decay signal, and is not sensitive to the magnetic field. We associate this feature with

the propagation of a coherent acoustic phonon generated at the surface (due to the short absorption depth (30-45 nm) of the 400 nm pump pulse) reaching the interface between the $BaTiO_3$-$BiFeO_3$ and the LSMO. The time it takes to reach to the interface is $t = L/v_s$, where L is the film thickness and v_s is the sound velocity of the solid solution.

While it is difficult to know the exact magnitude of acoustic sound velocity in the $BaTiO_3$-$BiFeO_3$ films, we do know that the Longitudinal Acoustic (LA) sound velocity is between 4.9 and 5.6 nm/ps in $BaTiO_3$ and is estimated to be in the range of 4.6-5.2 nm/ps in $BiFeO_3$.[48] Therefore, in our samples, it is not unreasonable to estimate that the sound velocity is in the range of 4.5-5 nm/ps. If the sample thickness is 80 nm, then the coherent phonon generated at the surface that should reach the $BaTiO_3$-$BiFeO_3$/LSMO interface in about 16-18 ps which is consistent with the experimental data.

In 80 nm thick film sample, we do not see the usual periodic modulation of the transient reflectivity due to coherent acoustic phonons, in contrast to the previous studies[30,38,44,48,49]. This is because the film thickness of 80 nm is too small. The acoustic pulse, generated at the surface, is already into the LSMO layer before a single oscillation can occur.

With an 800 nm for probe pulses, using the speed of sound (v_s) to be 4.5 nm/ps and an index of refraction of 2.5 (between $BiFeO_3$ and $BaTiO_3$ for 800 nm), we would predict $T = \lambda_{probe}/(2v_s n) = 36$ ps. Considering this fact, the strain pulse has left the $BaTiO_3$-$BiFeO_3$ in 16 ps, before even half a cycle of oscillation for the CP; therefore we do not see any oscillations and the carrier relaxation is the dominant feature. We also note that the application of external magnetic field modified the reflectivity traces only modestly for the 80-nm thick sample.

As shown in Fig. 6, among the films studied here, only the 660 nm $BaTiO_3$-$BiFeO_3$ film (and also the nanorods) showed a clear sinusoidal modulation in the transient reflectivity characteristic of coherent acoustic phonons (and also known as Brillouin oscillations). These types of oscillations have been observed in many systems including GaP layers grown on Si(001)[50]. All the data at 100 K was collected with a 400 nm pump at 2 mW power incident on the sample and 800 nm probe at less than 10 μW power. This result implies the 800 nm probe pulse can penetrate deep into the sample and detect the CPs as propagating strain pulses in the structure. Lowering temperature to reduce the damping of the phonon modes was also key to observing the CPs.[51,52] In this sample, we see a distinct bump in the signal at around 150 ps and the time is again consistent with the sound velocity in the
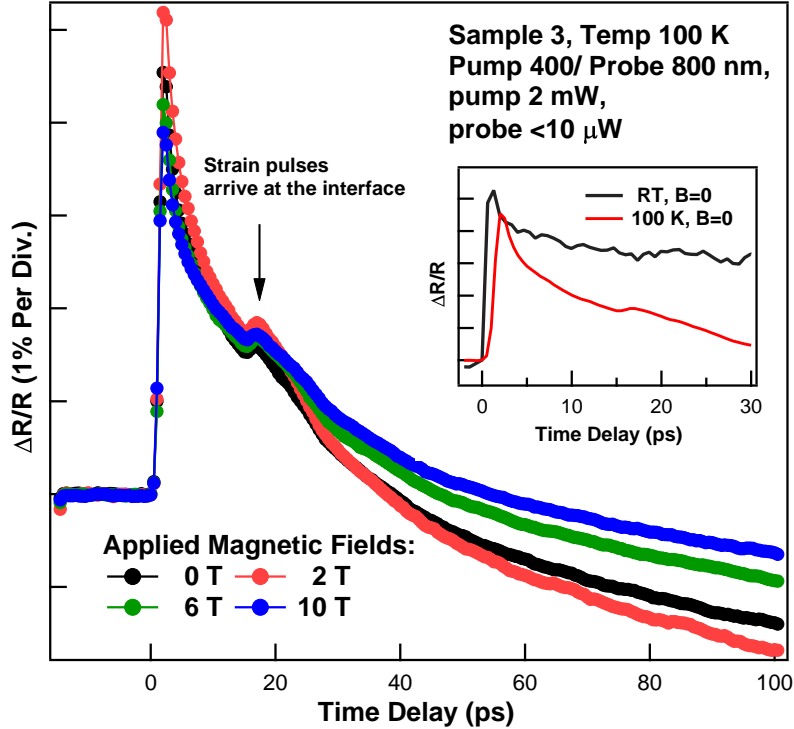
FIG. 5. TRDR for Sample 3 at 100 K for different external magnetic fields. The strain pulses arrive at the interface at ~ 20 ps and CP oscillations are not observed in this sample likely due to the response being dominated by carrier relaxation in the region < 20 ps where we would expect to observe them. The inset compares the reflectivity response of Sample 3 at room temperature (RT) and 100 K, both without applying an external magnetic field (B=0). At 100 K, the carrier-induced change in the refractive index could be responsible for the change in the sign of $\Delta R/R$.[43]

$BaTiO_3$-$BiFeO_3$ in the range of 4.5-5.0 nm/ps. The bump arises when the acoustic phonon generated at the surface reaches the interface with the LSMO layer. We should note that the reflection of the strain pulses at the interface is negligible since the acoustic impedances between the $BaTiO_3$-$BiFeO_3$ and LSMO are similar.

The period of the Brillouin oscillation (for normal incidence) is given by $T = \lambda_{probe}/(2v_s n)$, where λ_{probe} is the wavelength of the probe light, v_s, the sound velocity and n, the refractive index. If we take the value of n=2.5, in between $BaTiO_3$ and $BiFeO_3$, this agrees well with the experimentally observed period. We note that we saw no such oscillation for the thinner $BaTiO_3$-$BiFeO_3$ film in Fig. 5, because the film thickness is too small. The acoustic pulse reaches the LSMO layer before oscillations can occur. As described earlier, the cycle of

the Brillouin oscillation, 36 ps, implies that the acoustic pulse would leave the 80-nm thick $BaTiO_3$-$BiFeO_3$ film before half a cycle of the sinusoidal oscillation, making it difficult to be observed as a distinct oscillation.

The frequency of the observed Brillouin oscillation (27 GHz) in our $BaTiO_3$-$BiFeO_3$ is comparable with the thin films of $BiFeO_3$ on $LaAlO_3$ substrate studied by Doig $et.$ al[38] but lower compared to the LA frequencies (ranging from 34-38 GHz) of $BiFeO_3$ single crystals studied by Ruello $et.$ al[49] and Lejman $et.$ $al.$[48] where the same pump/probe wavelengths (400/800 nm) as our experimental schemes were used.

C.   Coherent Dynamics in $BaTiO_3$-$BiFeO_3$ Nano-rods

By lowering the temperature to 100 K, using the same experimental conditions for the films, we observed complex dynamics, including CPs propagation along the long axis of the rods. In Fig. 7(a) we present the TRDR of $BaTiO_3$-$BiFeO_3$ nano-rods taken at magnetic fields from $0-10$ T. The pump pulse was fixed at 400 nm with 2 mW of power and the probe at 800 nm with the power ~ 10 μW. Similar to our results for the 660 nm thick $BaTiO_3$-$BiFeO_3$ film, we observe a sudden change in $\Delta R/R$ (a bump) at ~ 120 ps time delay, when coherent longitudinal acoustic phonons generated at the surface of the $BaTiO_3$-$BiFeO_3$ nano-rods reached the interface between the $BaTiO_3$-$BiFeO_3$ and the Pt. The time delay of the bump ~ 120 ps (the time that the acoustic pulse entering the Pt layer) is again consistent with the propagation of a coherent acoustic phonon with a longitudinal sound velocity of 4.5-5.0 nm/ps. Focusing on Fig. 7(a), we observe two oscillation frequencies in the TRDR; the higher frequency oscillation (33 GHz), occurs only before the longitudinal acoustic mode encounters the interface and arises from the CP propagating in $BiFeO_3$.[38,44,49] The lower frequency (8.1 GHz) in Fig. 7(b), is very close to that of a theoretically predicted magnon frequency expected for 800 nm probe in $BiFeO_3$[38], where de Sousa $et.$ al[53] by solving the Landau-Lifshitz equations, mapped the low frequency magneto-static spin wave dispersion for a $BiFeO_3$ film.

If this coherent oscillation is caused by the magnons, then it does not significantly increase in strength with magnetic fields.[54] In addition, this mode can not be seen until after the coherent phonon travels from the surface, to reach the interface. Matching all traces at the negative time delay in Fig. 7(c), we can see only a small variation in the observed TRDR
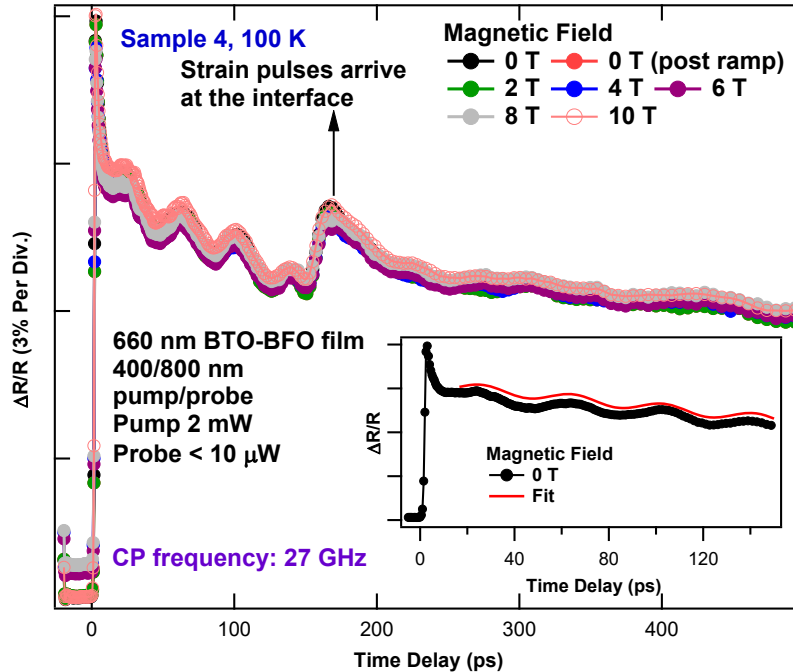
FIG. 6. Transient reflectivity for sample 4 at 100 K for different external magnetic field. We were able to detect CPs, corresponding to an LA phonon frequency of ~ 27 GHz. We observed no magnetic field dependence in the CP oscillations and the reproducibility of the observation at zero field, was confirmed by a post ramp trace, at the end. The feature at 170 ps represents the time for the strain pulses to reach to the interface. The inset shows the dynamics for the first 140 ps at zero magnetic field and the fit to the CP oscillations is to guide the eye. Note: The labels BTO-BFO refer to $BaTiO_3$-$BiFeO_3$ and the arrow shows the time that strain pulses arrive at the interface.

as a function of magnetic field, for the first 50 ps of the dynamics.

Talbayev *et. al* showed the sensitivity of the rocking magnon mode frequency to external magnetic fields in $Ba_{0.6}Sr_{1.4}Zn_2Fe_{12}O_{22}$ (BSZFO)[55]; on the other hand, in an earlier study on $BiFeO_3$ by Doig *et al.*[38], no shift in the frequency of the magnon mode was observed by applying small magnetic fields (0.5 T) to unpin the AFM spin cycloid.[38] The static ME coupling in BFO is weak as the FE and AFM orders originate from different ions and the
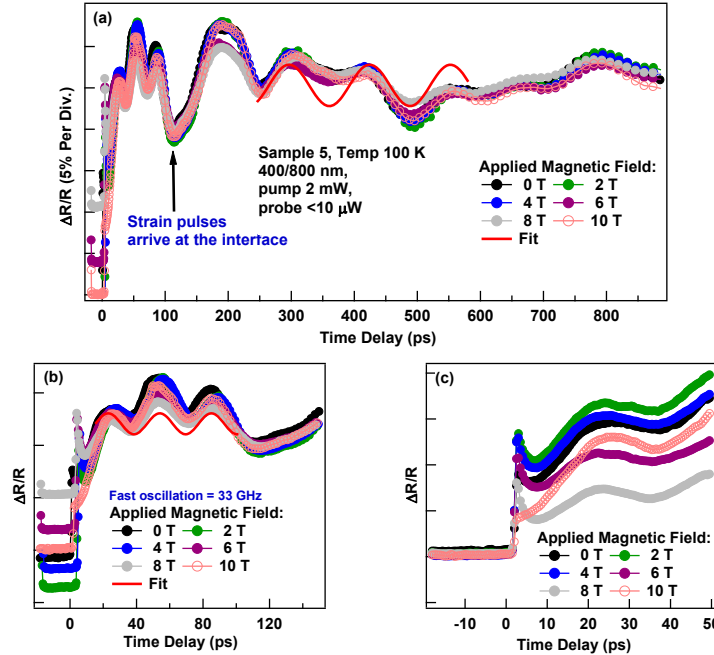
FIG. 7. a) The magnetic field dependence of TRDR and CPs in nano-rods (sample 5) at 100 K showing nearly periodic modulations at two different frequencies, 33 and 8.1 GHz. This lower frequency mode (8.1 GHz) is very close to the theoretically predicted magnon frequency.[38] Panels a-c) show the same traces with different x ranges and y offsets. In panel (c) matching the traces at the negative delays and focusing on the first 50 ps, a weak magnetic field dependence was noted. The fits to the CP oscillations are shifted for clarity and are the guides to the eye. Note: The labels BTO-BFO refer to $BaTiO_3$-$BiFeO_3$ and the arrow shows the time that strain pulses arrive at the interface.

presence of spin cycloid does not allow for a linear ME effect but the presence of a strong magnetic field (20 T, expected in case of $BiFeO_3$) can suppress the cycloid, to establish a linear ME effect.[56]

For a magnon in a simple AFM or FM an increase in frequency with applied magnetic field would be expected[54]. For example, in BSZFO at 0.1 T a distinct oscillatory response appears and further increase of the field leads to an increase in the oscillation period. At 1.2 T, in the collinear ferromagnetic phase, the oscillatory response changes and almost disappear at 2.5 T.[55] This fact demonstrates that magnon frequency can be sensitive to both the intensity of the external field and the fine details of the magnetization in the sample. In the case of our

newly developed nano-rods, more extensive studies are required to probe the interaction of the external magnetic fields and optically generated coherent oscillations.

We note that there is an interesting effect that might lead to a second possible origin of the slower oscillation. It could be related to the propagation of the strain pulses into the 100 nm thick Pt below the nano-rods, as shown in Fig. 2(b). The propagation of the CP deep into the Pt layer can not be detected by the optical probe pulse since the probe pulse can not penetrate into the Pt owing to its large extinction coefficient at 800 nm (4.148) which is equivalent to an absorption depth of 15 nm, similar to most metals. However, the differential reflectivity would be sensitive to the strain pulse at the interface. One possible explanation could be that the strain pulse in the 100 nm Pt layer is undergoing multiple reflections off of the Si substrate and coming back to the $BaTiO_3$-$BiFeO_3$/LSMO/Pt interface. This fact could result in a quasi-periodic modulation at the interface and lead to the observed oscillations in the differential reflectivity. It is also possible, that one is seeing reflections between the BTO/BFO -Pt layer and the surface or some combination of the two.

Why then did not we see reflections of the strain pulses in the previous samples? We note that for the previous samples, the $BaTiO_3$-$BiFeO_3$ was on LMSO and then on STO. The acoustic impedance $Z = \rho v_s$ (here ρ is the density and v_s is the sound velocity) for the layers is almost equal and hence, there is little acoustic reflection from the interfaces. For $BaTiO_3$-$BiFeO_3$ we estimate an acoustic impedance Z = 38 (in units of $g/cm^3 \ nm/ps$) based on densities of $BiFeO_3$, $\rho = 9.15 \ g/cm^3$ and $BaTiO_3$, $\rho = 6.02 \ g/cm^3$, taking a weighted average (0.75 to 0.25), using a sound velocity 4.5 nm/ps. For LSMO, the acoustic impedance is Z=42 (using $\rho = 6.5 \ g/cm^3$ and a sound velocity 6.5 nm/ps.) For STO, we find Z = 40 (using $\rho = 5.11 \ g/cm^3$ and $V_s = 7.8 \ nm/ps$. Since the acoustic impedances are nearly equal, we find little reflection at the interfaces, (less than 1%).

However, for the nano-rod samples, which are on a Pt layer, the density of Pt is much larger than Si (and also the $BaTiO_3$-$BiFeO_3$ density) and leads to a large acoustic mismatch at the interface. For instance, for the longitudinal modes, the acoustic impedance for Pt is $85 \ g/cm^2 - sec \times 10^5$ compared to that for Si which is $20 \ g/cm^2 - sec \times 10^5$. As a result, the reflectivity at the Si-Pt interface represented as: $R = \left| \frac{Z_{Pt}-Z_{Si}}{Z_{Pt}+Z_{Si}} \right|^2$, is about 0.4. It is possible that one is getting multiple reflections in the Pt layer at the two interfaces (or possible from the first interface and the surface). If this were the case, one would get pulses at a frequency given by: $f = v_{Pt}/200$ nm. Since the initial strain generated by the photoexcited

carriers at the surface is fairly wide (two times the 30-45 nm absorption depth, which is significant compared to the width of the Pt layer, the "echo" pulses will be fairly broad. For a longitudinal sound mode in Pt (with velocity 3.96 nm/ps) this would correspond to a come-back time of 51 ps corresponding to a frequency of 19.8 GHz. This seems a bit too slow to explain the features. However, it is interesting to note that for the Transverse Acoustic (TA) mode in Pt, this would correspond to a return time of 120 ps corresponding to a frequency of 8.35 GHz, very close to the observed frequency in this work. In a single crystal of $BiFeO_3$ for one of the grain sizes, Lejman *et. al* reported a TA frequency of ~ 10 GHz.[48]

How would one generate the TA mode in the Pt system? We conjecture that since the nano-rods do not cover the entire Pt interface, when the LA modes in the nano-rods reach at the interface, they can excite TA modes through the non-uniform longitudinal strain at the surface which gives rise to a shear strain. That is, there is a net shear strain at the interface which could be responsible for generating the TA modes. While both the magnon and reflecting TA phonon mode in Pt are intriguing explanations for the observation of the 8.1 GHz feature, it is clear that additional studies will be needed to more accurately elucidate and verify the origin of this feature.

IV. Conclusions

We have studied the dynamical properties of a variety of $BaTiO_3$-$BiFeO_3$ films and nano-rods using ultrafast TRDR spectroscopy. Adding $BaTiO_3$ to $BiFeO_3$ can reduce the conductivity of the mixture and improve the multiferroic behavior. This is an interesting lead-free system and our ultrafast optical measurements of these less explored systems provided insight into some of the dynamical properties of these systems.[2] Our results can provide insight to employ these complex materials for applications such as optical switching in multiferroics.

Our main results are the detection of coherent acoustic phonons in the samples (both films and nanorods) at lower (100 K) temperatures. The coherent phonons are generated near the surface and are the consequence of the short absorption length of the photoexcited carriers for the 400 nm pump pulse. In thin samples, we do not see the usual oscillations in the differential reflectivity of the coherent phonons because the films are too thin. The acoustic strain pulse has traveled through the entire $BaTiO_3$-$BiFeO_3$ film and into the LSMO

layer before any oscillations can occur. Instead, in these thin film samples, we distinctly see a sudden change in the differential reflectivity (a bump) when the strain pulse enters into the LSMO layer. From the thickness of the $BaTiO_3$-$BiFeO_3$ films, we can estimate the speed of sound in the film. We find a speed of sound (depending on the film) in the range of 4.5 - 5.0 nm/ps, which is comparable to sound speeds in $BiFeO_3$ and slightly below the sound speeds in $BaTiO_3$.

In thicker films, we saw the usual coherent phonon oscillations from the acoustic strain pulse propagating in the $BaTiO_3$-$BiFeO_3$ layer and then a similar bump in the differential reflectivity when the strain pulse entered the LSMO layer. From the period of the initial oscillation and using the sound velocity determined by the arrival of the strain pulse at the LSMO layer, we estimate the index of refraction of our $BaTiO_3$ to $BiFeO_3$ to be 2.5.

In the nanorod samples, we observed coherent phonon oscillations similar to the $BaTiO_3$-$BiFeO_3$ films at the earliest times. In addition, we saw oscillations (with a different period) at time scales longer than the time it takes for the acoustic strain pulse to reach the Pt layer. This is somewhat perplexing since the optical probe pulse can not penetrate too far into the Pt layer before it is attenuated. We postulated that the oscillations could be related to a coherent magnon or possibly from multiple reflections with the Pt layer since Pt has a much greater acoustic impedance than the other materials leading to reflections of the acoustic pulse at the Pt interfaces. Further study will be needed to determine the origin of these oscillations.

In addition to the coherent phonon oscillations and effects, the overall background of the differential reflectivity changed with time. We attributed this change to the dynamics of the photoexcited carriers. The decay signal could be quantitatively explained by the diffusion of the photoexcited carriers away from the surface and that the ambipolar diffusion constant was less than 1-2 cm^2/s.

While CPs are typically used to provide detailed spectroscopy information and characterize surfaces and buried interfaces,[50] it has recently been demonstrated that dynamical strains in Surface Acoustic Wave (SAW) devices can interact with spins in silicon carbide.[57] This suggests that our approach of employing ultrafast optical generation of the strain, offers a potentially better means of generating the dynamic strain that can bypass the need to fabricate a SAW device and allow for higher frequencies and faster manipulation. For future applications, the ability to generate strain via ultrafast optics offers the intriguing

possibility of dynamically manipulating the strain, opening the possibility of creating a new class of devices. In this fashion, the strain is manipulated in time and one can generate and control the photo-generated CPs to ultimately control electric, magnetic and strain fields which can lead to revolutionary new devices.[58–61] Furthermore, a material system where the ME coupling can be enhanced, could be a powerful method for tuning coherent modes such as magnons.

1 Min Gyu Kang, Seul-Yi Lee, Deepam Maurya, Christopher Winkler, Hyun-Cheol Song, Robert B. Moore, Mohan Sanghadasa, and Shashank Priya, Advanced Functional Materials, **27**, 1701542 (2017).

2 S.-C. Yang, A. Kumar, V. Petkov, and S. Priya, J. of Appl. Phys., **113**, 144101 (2013).

3 W. Eerenstein, N. D. Mathur, and J. F. Scott, Nature, **442**, 759 (2006).

4 T. Zhao, A. Scholl, F. Zavaliche, K. Lee, M. Barry, A. Doran, M. P. Cruz, Y.H. Chu, C. Ederer, N. A. Spaldin, R. R. Das, D. M. Kim, S. H. Baek, C. B. Eom, and R. Ramesh, Nat Mater, **5**, 823, (2006).

5 M. Fiebig, Thomas Lottermoser, Dennis Meier, and Morgan Trassin, Nat Rev, **1**, 16046 (2016).

6 Pankaj Sharma, Qi-Zhang, Daniel Sando, Chi-Hou Lei, Yunya Liu, Jiangyu Li, Valanoor Nagarajan, and Jan Seidel, Science Advances, **3**(6), e1700512 (2017).

7 Ji-Hoon Jeon, Ho-Young Joo, Young-Min Kim, Duk-Hyun Lee, Jin-Soo Kim, Yeon-Soo Kim, Taekjib Choi, and Bae-Ho Park, Sci. Rep., **6**, 23299 (2016).

8 T. Choi, S.Lee, Y. J. Choi, V.Kiryukhin, and S.-W. Cheong, Science, **324**, 63 (2009).

9 S. Y. Yang, L. W. Martin, S. J. Byrnes, T. E. Conry, S. R. Basu, D. Paran, L. Reichertz, J. Ihlefeld, C. Adamo, A. Melville, Y.-H. Chu, C.-H. Yang, J. L. Musfeldt, D. G. Schlom, J. W. Ager, and R. Ramesh, App. Phys. Lett., **95**, 062909 (2009).

10 D. Maurya, A. Charkhesht, S. K. Nayak, F-C. Sun, D. George, A. Pramanick, M-G. Kang, H-C. Song, M. M. Alexander, D. Lou, G. A. Khodaparast, S. P. Alpay, N. Q. Vinh, and S. Priya, Phys. Rev. B, **96**, 134114 (2017).

11 M. A. Meeker, S. Kundu, D. Maurya, Min-Gyu Kang, A. Sosa, R. R. H. H. Mudiyanselage, M. Clavel, S. Gollapudi, M. K. Hudait, S. Priya, G. A.Khodaparast, Optical Materials, **73**, 793 (2017).

12 R. Ramesh and N. A. Spaldin, Nat Mater, **6**, 21 (2007).

13 Ce-Wen Nan, M. I. Bichurin, Shuxiang Dong, D. Viehland, and G. Srinivasan, J. Appl. Phys., **103**, 031101 (2008).

14 Manuel Bibes and Agnés Barthélémy, Nature Materials, **7**, 425 (2008).

15 S. Fusil, V. Garcia, A. Barthélémy, and M. Bibes, Annu. Rev. Mater. Res., **44**, 91 (2014).

16 X. Yang, Z. Zhou, T. Nan, Y. Gao, G. M. Yang, M. Liu and N. X. Sun, J. Mater. Chem. C, **4**,

234 (2016).

[17] D. S. Rana, I. Kawayama, K. Mavani, K. Takahashi, H. Murakami, and M. Tonouchi, Adv. Mater., **21**, 2881 (2009).

[18] Jan Seidel, Deyi Fu, Seung-Yeul Yang, Esther Alarcón-Liadó, Junqiao Wu, Ramamoorthy Ramesh, and Joel W. Ager, Phys. Rev. Lett., **107**, 126805 (2011).

[19] Dawei Cao, Chunyan Wang, Fengang Zheng, Wen Dong, Liang Fang, and Mingrong Shen, Nano Lett., **12**, 2803 (2012).

[20] A. E. Bruchhausen, N. D. Lanzillotti-Kimura, B. Jusserand, A. Soukiassian, L. Xie, X. Q. Pan, T. Dekorsy, D. G. Schlom, and A. Fainstein, Phys. Rev. Mate., **2**, 106002 (2018).

[21] A. Soukiassian, W. Tian, D. A. Tenne, X. X. Xi, and D. G. Schlomb, N. D. Lanzillotti-Kimura, A. Bruchhausen, and A. Fainstein, H. P. Sun and X. Q. Pan, A. Cros and A. Cantarero, App. Phys. Lett., **90**, 042909 (2007)

[22] N. D. Lanzillotti-Kimura, A. Fainstein, B. Perrin, B. Jusserand, A. Soukiassian, and D. G. Schlom, Phys. Rev. Lett. **104**, 187402 (2010).

[23] P. A. Fleury and P. D. Lazay, Phys. Rev. Lett., **26**, 1331 (1971).

[24] J. H. Haeni, P. Irvin, W. Chang, R. Uecker, P. Reiche, Y. L. Li, S. Choudhury, W. Tian, M. E. Hawley, B. Craigo, A. K. Tagantsev, X. Q. Pan, S. K. Streiffer, L. Q. Chen, S. W. Kirchoefer, J. Levy, and D. G. Schlom, Nature London, **430**, 758 (2004).

[25] J. B. Neaton and K. M. Rabe, Appl. Phys. Lett., **82**, 1586 (2003).

[26] K. J. Choi, M. Biegalski, Y. L. Li, A. Sharan, J. Schubert, R. Uecker, P. Reiche, Y. B. Chen, X. Q. Pan, V. Gopalan, L.-Q. Chen, D. G. Schlom, and C. B. Eom, Science **306**, 1005 (2004).

[27] Tae-Jin Park, Georgia C. Papaefthymiou, Arthur J. Viescas, Yongjae Lee, Hongjun Zhou, and Stanislaus S. Wong, Phys. Rev. B, **82**, 024431 (2010).

[28] B. Madon, H. Byul Kang, M. Gyu Kang, D. Maurya, B. A. Magill, M. J. P. Alves, J.-E. Wegrowe, H.-J. Drouhin, S. Priya, and G. A. khodaparast , AIP Advances, **8** (10), 105034 (2018).

[29] C. J. Cook, S. Khan, G. D. Sanders, X. Wang, D. H. Reitze, Y. D. Jhod, Y.-W. Heoe, J.-M. Eriee, D. P. Nortone, and C. J. Stanton, Proc. of SPIE, **7603**, 760304 (2010).

[30] B. A. Magill, K.-D. Park, Y. Zhou, A. Chopra, D. Maurya, S. Priya, M. Raschke, A. Belyanin, C. J. Stanton, G. A. Khodaparast, Energy Harvesting and Systems, **3**, 229 (2016).

[31] B. A. Magill, M. Bishop, S. A. McGill, Y. Zhou, A. Chopra, H.-C. Song, C. J. Stanton, S. Priya,

G. A. Khodaparast, Proc. of SPIE, **9551**, 95510T (2015).

32 R. Safi, H. Shokrollahi, Progress in Solid State Chemistry, **40**, 6 (2012).

33 T-J. Park, G. C. Papaefthymiou, A. J. Viescas, A. R. Moodenbaugh, S. S. Wong, Nano Lett.,
    7, 766 (2007).

34 T-J. Park, G. C. Papaefthymiou, A. J. Viescas, Y. Lee, H. Zhou, S. S. Won, Phys. Rev. B, **82**,
    024431 (2010).

35 T. Zhao, A. Scholl, F. Zavaliche, K. Lee, M. Barry, A. Doran, M. P. Cruz, Y. H. Chu, C. Ederer,
    N. A. Spaldin, R. R. Das, D. M. Kim, S. H. Baek, C. B. Eom, R. Ramesh, Nature Materials,
    5, 823 (2006).

36 H. Béa, M. Bibes, S. Petit, J. Kreisel, and A. Barthélémy, Philosophical Magazine Letters, **87**,
    165 (2007).

37 D. Sando, A. Agbelele, D. Rahmedov, J. Liu, P. Rovillain, C. Toulouse, I. C. Infante, A. P.
    Pyatakov, S. Fusil, E. Jacquet, C. Carrétéro, C. Deranlot, S. Lisenkov, D. Wang, J-M. Le Breton,
    M. Cazayous, A. Sacuto, J. Juraszek, A. K. Zvezdin, L. Bellaiche, B. Dkhil, A. Barthélémy, and
    M. Bibes, Nature Materials, **12**, 641 (2013).

38 K. I. Doig, F. Aguesse, A. K. Axelsson, N. M. Alford, S. Nawaz, V. R. Palkar, S. P. P. Jones,
    R. D. Johnson, R. A. Synowicki, and J. Lloyd-Hughes, Phys. Rev. B, **88**, 094425 (2013).

39 Jian-Ping Zhou, Rui-Juan Xiao, Yu-Xiang Zhang, Zhenhua Shi, and Gang-Qiang Zhu, J. Mater.
    Chem. C, **3**, 6924 (2015).

40 Akira Imai, Xuan Cheng, Huolin. L. Xin, Eugene A. Eliseev, Anna N. Morozovska, Sergei V.
    Kalinin, Ryota Takahashi, Mikk Lippmaa, Yuji Matsumoto, and Valanoor Nagarajan, ACS
    Nano, **7** 11079, (2013).

41 Zuanming Jin, Yue Xu, Zhengbing Zhang, Gaofang Li, Xian Lin, Guohong Ma, Zhenxiang
    Cheng, and Xiaolin Wang, Appl. Phys. Lett., **100**, 071105 (2012).

42 Eiichi Matsubara, Takeshi Mochizuki, Masaya Nagai, Toshimitsu Ito, and Masaaki Ashida, Jpn.
    J. Appl. Phys. **54**, 092201 (2015).

43 Nathan P. Wells, Paul M. Belden, Joseph R. Demers, and William T. Lotshaw, J. of Appl,
    Phys., **116**, 073506 (2014).

44 L. Y. Chen, J. C. Yang, C. W. Luo, C. W. Laing, K. H. Wu, Appl. Phys. Lett., **101**, 041902
    (2012).

45 S. Zollner, K.D. Myers, J.M. Dolan, D.W. Bailey, C.J. Stanton, Thin Solid Films, **313-314**,

568 (1998).

[46] A. Kumar, R. C. Rai, N. J. Podraza, S. Denev, M. Ramirez, Y.-H. Chu, L. W. Martin, J. Ihlefeld, T. Heeg, J. Schubert, D. G. Schlom, J. Orenstein, R. Ramesh, R. W. Collins, J. L. Musfeldt and V. Gopalan., Appl. Phys. Lett., **92**, 121915 (2008).

[47] Amlan Kumar Basak, Hrvoje Petek, Kunie Ishioka, Evan M. Thatcher, and Christopher J. Stanton, Phys. Rev. B, **91**, 125201 (2015).

[48] M. Lejman, G. Vaudel, I. C. Infante, P. Gemeiner, V. E. Gusev, B. Dkhil, and P. Ruello, Nature Communications, **5**, Article number: 4301 (2014).

[49] P. Ruello, T. Pezeril, S. Avanesyan, G. Vaudel, V. Gusev, I. C. Infante, B. Dkhil, App. Phys. Lett., **100**, 212906 (2012).

[50] Kunie Ishioka, Kristina Brixius, Andreas Beyer, Avinash Rustagi, Christopher J. Stanton, Wolf-gang Stolz, Kerstin Volz, Ulrich Höfer, and Hrvoje Petek, Applied Physics Letters **108**, 051607 (2016).

[51] R. Palai, J. F. Scott, and R. S. Katiyar, Phys. Rev. B **81**, 024115 (2010).

[52] Muneaki Hase, Kunie Ishioka, Jure Demsar, Kiminori Ushida, and Masahiro Kitajima, Phys. Rev. B **71**, 184301 (2005).

[53] Rogerio de Sousa and Joel E. Moore, Appl. Phys. Lett., **92**, 022514 (2008).

[54] J. van Kranendonk and J. van Vleck, Rev. Mod. Phys., **30**, 1 (1958).

[55] D. Talbayev, S. A. Trugman, A. V. Balatsky, T. Kimura, A. J. Taylor, and R. D. Averitt, Phys. Rev. Lett., **101**, 097603 (2008).

[56] Y. F. Popov, A. M. Kadomtseva, S. S. Krotov, D. V. Belov, G. P. Vorobév, P. N. Makhov, and A. K. Zvezdin, Low Temp. Phys., **27**, 478 (2001).

[57] Samuel J. Whiteley, Gary Wolfowicz, Christopher P. Anderson, Alexandre Bourassa, He Ma, Meng Ye , Gerwin Koolstra, Kevin J. Satzinger , Martin V. Holt, F. Joseph Heremans, Andrew N. Cleland, David I. Schuster, Giulia Galli and David D. Awschalom, Nature **15** 490 (2019).

[58] K. J. Satzinger, Y. P. Zhong, H.-S. Chang, G. A. Peairs, A. Bienfait, M.-H. Chou, A. Y. Cleland, C. R. Conner, E. Dumur, J. Grebel, I. Gutierrez, B. H. November, R. G. Povey, S. J. Whiteley, D. D. Awschalom, D. I. Schuster, A. N. Cleland, Nature, **563**, 661, 2018.

[59] J. Wang, G. A. Khodaparast, J. Kono, A. Oiwa, and H. Munekata, Journal of Modern Optics, **51**, 2771 (2004).

[60] J. Wang, C. Sun, Y. Hashimoto, J. Kono, G. A. Khodaparast, L. Cywinski, L. J. Sham, G. D.

Sanders, C. J. Stanton, and H. Munekata, J. Phys.: Condens. Matter, **18**, R501 (2006).

[61] Michael K. Yakes, Cory D. Cress, Joseph G. Tischler, and Allan S. Bracke, ACS Nano, **4**, 3877 (2010).